

## PROPER MOTIONS AND DISTANCES OF H<sub>2</sub>O MASER SOURCES. I. THE OUTFLOW IN ORION-KL

R. GENZEL,<sup>1</sup> M. J. REID,<sup>1</sup> J. M. MORAN,<sup>1</sup> AND D. DOWNES<sup>2</sup>

*Received 1980 June 23; accepted 1980 October 1*

### ABSTRACT

We report the measurement of relative proper motions of H<sub>2</sub>O maser features at 22 GHz with VLBI methods. In the H<sub>2</sub>O source in Orion-KL, the transverse motions are typically a few milli-arcsec per year. We interpret these as kinematic motions of compact cloudlets of masing gas. The data from Orion show a large scale outflow of maser features at 18 km s<sup>-1</sup> from a common origin situated within 5" of the compact infrared source IRC2. We suggest that all outflow phenomena seen in molecular lines with a velocity spread of approximately ±20 km s<sup>-1</sup> are associated with the luminous, heavily obscured infrared source IRC2 and *not* with the BN object.

In addition to the "18 km s<sup>-1</sup> flow," there is a second, *high velocity* (30–100 km s<sup>-1</sup>) outflow with approximately the same centroid. This high velocity flow may come from a different source, such as BN, or, more likely, may also be associated with IRC2.

Radiation pressure from IRC2 may not be adequate to drive the outflow of ~10<sup>-3</sup>M<sub>⊙</sub> yr<sup>-1</sup>. More likely, the loss of rotational, magnetic, or gravitational energy of a massive star in the last stages of formation accounts for the high mass loss over a time scale of 10<sup>3</sup>–10<sup>4</sup> years. Observations of other H<sub>2</sub>O maser sources in the Galaxy suggest that such mass loss phenomena may be common in many regions of active star formation.

We discuss two different methods for determining *distances* from a comparison of proper motions and radial velocities. We estimate the distance of Orion-KL to be 480 ± 80 pc.

*Subject headings:* infrared: sources — interferometry — interstellar: molecules — masers — nebulae: individual — stars: formation — stars: mass loss

### I. INTRODUCTION

Strong H<sub>2</sub>O maser sources in regions of active star formation show two types of emission: strong, *low velocity* lines with a range ±10 km s<sup>-1</sup> about the radial velocity of the associated molecular cloud, and weak, *high velocity* features over ±10 to ±250 km s<sup>-1</sup> around the low velocity emission (Genzel and Downes 1977). The most likely interpretation of the H<sub>2</sub>O spectra is kinematic, that is, the observed radial velocities correspond to actual motions of the maser cloudlets (Strel'nitskii and Syunyaev 1972). The large velocity dispersions, together with the spatial distributions of the maser features mapped by VLBI, suggest that H<sub>2</sub>O masers are associated with as yet unexplained mass loss phenomena in the last stages of the formation of massive stars (Walker *et al.* 1977, 1978; Genzel *et al.* 1978, 1979*a*). However, nonkinematic explanations of the high velocity emission have been suggested by several authors (Radhakrishnan, Goss, and Bhandari 1975; Montes 1977; Fernandez and Reinisch 1978;

Burdjuzha, Charugin, and Tomosov 1979). It has been proposed, for example, that Raman scattering or inelastic plasma scattering could transfer power from the intense low velocity lines into "images" at other frequencies.

If the observed radial velocities are kinematic, the maser features should move on the sky with respect to each other, with proper motions corresponding to the spread in radial velocities. A measurement of relative proper motions of maser features, therefore, can be used to decide between a kinematic or nonkinematic origin of the observed velocities. Furthermore, proper motions of many maser features give the three-dimensional velocity field, and—if the kinematics are simple—the three-dimensional structure of the source. Finally, a comparison of the radial and transverse motions (*Statistical Parallax* or *Expanding Cluster Parallax*) provides a direct estimate of the distance to the maser source.

In 1977, we started a series of six VLBI experiments to measure the relative proper motions of maser features in three strong H<sub>2</sub>O sources in regions of star formation. The participating stations were the 22 m telescope of the Crimean Astrophysical Observatory, the 20 m telescope of the Onsala Space Observatory,

<sup>1</sup>Harvard/Smithsonian Center for Astrophysics, Cambridge, Massachusetts.

<sup>2</sup>Institut de Radio Astronomie Millimetrique, Grenoble, France, and Max Planck Institut für Radioastronomie, Bonn, West Germany.

the 100 m telescope of the Max Planck Institute for Radio Astronomy, the 37 m telescope of the Haystack Observatory, the 43 m telescope of the National Radio Astronomy Observatory<sup>3</sup>, and the 40 m telescope of the Owens Valley Radio Observatory. In this paper, we report the results on Orion-KL. In two companion papers, we discuss the results in W51MAIN (Genzel *et al.* 1981, hereafter Paper II) and in W51NORTH (Schneps *et al.* 1981, hereafter Paper III).

## II. OBSERVATIONS AND DATA REDUCTION

### a) Observing Method

Individual H<sub>2</sub>O maser features at 22 GHz vary on time scales of a few weeks to one year and may have lifetimes of only a few years (e.g., Haschick, Burke, and Spencer 1977; Little, White, and Riley 1977). High velocity masers are particularly unstable. Therefore, measurements of the motions of individual features must be accomplished within a time span of one or two years. The relative positional accuracy,  $\Delta\theta$ , needed to measure a proper motion in a source at distance  $D$ , transverse velocity  $v$ , over a time span  $\Delta t$  is

$$\left[ \frac{\Delta\theta}{\text{milli-arcsec}} \right] = 0.14 \left[ \frac{D}{\text{kpc}} \right]^{-1} \left[ \frac{\Delta t}{y} \right] \left[ \frac{v}{\text{km s}^{-1}} \right]. \quad (1)$$

In Orion-KL ( $D=0.5$  kpc),  $\Delta\theta$  is a few milli-arcsec for  $v=10$  km s<sup>-1</sup> and  $\Delta t=2y$ . In W51MAIN, at a distance of 7 kpc, the measurement accuracy has to be an order of magnitude more stringent.

In our experiments, the data were recorded on videotape with the Mark II VLBI system (Clark 1973). In order to cover H<sub>2</sub>O maser features over a total range of  $\sim 100$  km s<sup>-1</sup> (7 MHz), we switched the recorded videoband (bandwidth=2 MHz) every second among four sky frequencies. We tracked sources from horizon to horizon to accurately determine the change of fringe rate or phase with interferometer hour angle. Relative positions of the maser features were obtained by multiple fringe rate and phase mapping (for details, see Moran 1976; Reid 1976; Reid *et al.* 1977; Giuffrida 1977; Walker *et al.* 1981). The positions of the maser components, measured with respect to a common reference feature, are given in Table 1. The observations on source were supplemented with OFF source observations to obtain total power spectra for internal calibration of the cross-correlation amplitudes. We also observed compact radio continuum sources every other hour to calibrate the time delays between telescopes.

<sup>3</sup>The National Radio Astronomy Observatory is operated by the Associated Universities, Inc., under contract with the National Science Foundation.

### b) Fringe Rate Analysis

A maser feature at a given velocity is often not a single point source but rather a blend of several point-like components at slightly different positions on the sky. The multiple fringe rate analysis can resolve such blends as long as the components are separated by more than the "fringe rate beam,"

$$\Delta\theta_{\text{FB}} = \frac{\lambda}{B\Omega_E T \cos \psi}, \quad (2)$$

where  $\lambda$  is the wavelength ( $\lambda_{\text{H}_2\text{O}}=1.3$  cm),  $B$  is the length of the equatorial component of the baseline,  $\Omega_E$  is the rotation rate of the Earth ( $7.3 \times 10^{-5}$  rad s<sup>-1</sup>),  $T$  is the integration time (typically 30 minutes), and  $\psi$  is the angle between the baseline vector and the direction to the source.

The fringe rate changes during a typical 30-minute scan by about 5%. The corresponding fringe rate beam can be severely distorted by this effect if the separation between a maser feature and the reference position is larger than 100–500 milli-arcsec. It is therefore necessary, first, to make a coarse map to locate the features, then to shift the interferometer phase center close to the positions of individual features or groups of features, and finally to analyze the residual fringe rates.

With a high signal-to-noise ratio, the best achievable accuracy of fringe rate positions is a small fraction of  $\Delta\theta_{\text{FB}}$ , typically one milli-arcsec on short baselines ( $B \sim 500$  km) and 100 micro-arcsec on intercontinental baselines ( $B \sim 5000$  km). There are, however, several systematic effects which degrade this accuracy:

1. Approximations and linear expansions in the current data reduction limit the accuracy of relative position measurements to  $\sigma_{\Delta\theta}/\Delta\theta \sim 10^{-5}$ . This applies to both fringe rate and phase analysis.

2. Maser features are sometimes blended on a scale size of less than the fringe rate beam ( $\leq 10$ –50 milli-arcsec), and a multiple fringe rate analysis will give a (useless) average position of the blended features. In practice, such blending can be recognized as a poor fit, or simply by inspection of raw amplitudes and phases.

### c) Phase Analysis

In theory, the accuracy of positions determined from an analysis of fringe *phases* is 2 orders of magnitude better than of fringe *rates*. The interferometer fringe spacing on intercontinental baselines is about 0.4 milli-arcsec, and the limiting positional accuracy due to signal-to-noise considerations is typically a few micro-arcsec. However, the phase analysis is susceptible to systematic errors. The relative fringe phase between two maser features at sky frequencies  $\omega$  and  $\omega'$ , which are separated by an angular distance  $\theta_X$  and  $\theta_Y$  on the

TABLE I  
RELATIVE POSITIONS OF H<sub>2</sub>O MASERS IN ORION-KL

LSR Radial Velocity [km s <sup>-1</sup> ]	1977 November <sup>d</sup>				1977 December <sup>e</sup>				1978 February <sup>f</sup>			
	$\Delta X^a$	$\sigma_{\Delta X}$	$\Delta Y^a$	$\sigma_{\Delta Y}$	$\Delta X$	$\sigma_{\Delta X}$	$\Delta Y$	$\sigma_{\Delta Y}$	$\Delta X$	$\sigma_{\Delta X}$	$\Delta Y$	$\sigma_{\Delta Y}$
-8	-8.039	1	1.906	15	-8.039	4	1.87	100	...	...	...	...
-7.5	...	...	...	...	-3.279	10	1.79	100	...	...	...	...
-6	...	...	...	...	-0.336	2	1.37	40	...	...	...	...
-4	2.794	6	7.80	100	2.788	2	7.61	80	2.786	6	7.49	90
-4	-3.714	1	3.728	15	-3.715	1	3.688	3	-3.716	1	3.693	2
1	-14.93	50	20.2	500	...	...	...	...	...	...	...	...
2.4	...	...	...	...	...	...	...	...	...	...	...	...
2.9	...	...	...	...	...	...	...	...	...	...	...	...
3	-0.885	1	2.223	15	-0.886	1	2.193	3	-0.886	1	2.192	6
4.3	-0.537	3	1.900	30	...	...	...	...	-0.538	2	1.884	20
4	...	...	...	...	...	...	...	...	...	...	...	...
2.8	...	...	...	...	...	...	...	...	...	...	...	...
4	6.722	1	20.408	15	6.721	2	20.435	40	6.720	1	20.382	10
4	6.730	1	20.418	15	6.730	1	20.420	30	6.732	1	20.372	5
2	5.408	6	10.753	40	...	...	...	...	5.414	2	10.724	14
5.5	...	...	...	...	...	...	...	...	...	...	...	...
6.5	...	...	...	...	-6.663	5	37.36	40	...	...	...	...
6.5	-3.785	1	-0.384	5	-3.786	1	-0.418	20	...	...	...	...
6	-3.105	2	-1.474	15	-3.126	16	-1.68	120	-3.102	2	-1.506	20
8.1	...	...	...	...	...	...	...	...	...	...	...	...
7	-0.759	2	-1.559	10	-0.759	2	1.518	30	...	...	...	...
8	-4.220	2	-1.198	10	-4.222	1	-1.231	5	...	...	...	...
8.4	...	...	...	...	...	...	...	...	...	...	...	...
8	-0.138	2	0.291	15	-0.140	1	0.266	5	-0.142	1	0.258	5
8.5	...	...	...	...	...	...	...	...	...	...	...	...
9.5	-7.718	2	-1.580	20	-7.717	1	-1.600	10	-7.715	2	-1.614	10
10	11.490	1	21.276	5	11.490	1	21.260	12	11.488	2	21.225	30
10.5	...	...	...	...	-3.026	5	-1.535	50	...	...	...	...
11	11.346	3	21.286	15	11.344	2	21.301	5	11.354	2	21.262	15
12	...	...	...	...	...	...	...	...	...	...	...	...
12.6	7.083	2	18.898	22	7.078	2	18.865	30	...	...	...	...
13	...	...	...	...	-3.086	15	-1.46	400	...	...	...	...
15	...	...	...	...	1.966	4	7.64	70	...	...	...	...
15.5	10.453	6	19.741	60	10.448	2	19.670	50	10.450	2	19.65	40
14.5	-8.640	2	-0.668	10	-8.641	2	-0.640	24	...	...	...	...
16	-8.287	1	-0.898	6	-8.288	2	-0.910	5	-8.288	2	-0.913	16
16	...	...	...	...	...	...	...	...	...	...	...	...
16	1.663	4	46.354	10	1.660	4	46.409	40	...	...	...	...
17.3	-3.633	1	-1.207	3	-3.636	2	-1.24	35	...	...	...	...
18	0	...	0	...	0	...	0	...	0	...	0	...
19	...	...	...	...	...	...	...	...	...	...	...	...
21	-4.170	3	2.266	20	-4.172	2	2.300	20	...	...	...	...
21.5	-0.067	8	0.091	50	-0.063	6	0.150	200	...	...	...	...
22	-7.077	5	45.347	15	-7.078	5	45.314	60	...	...	...	...
23.5	...	...	...	...	...	...	...	...	...	...	...	...
23	...	...	...	...	-9.699	2	-1.166	35	...	...	...	...
25	-7.335	2	-1.569	10	-7.334	2	-1.603	20	...	...	...	...
25	0.264	2	-0.044	10	0.264	1	-0.048	5	...	...	...	...
27	-3.287	1	1.931	5	-3.288	1	1.932	5	-3.288	2	1.916	12
46	-7.238	1	-1.170	6	-7.239	3	-1.140	60	...	...	...	...
61	...	...	...	...	15.805	2	0.010	10	15.813	2	0.017	25
64	15.791	2	0.100	15	15.789	2	0.070	10	15.799	2	0.060	10
69	...	...	...	...	15.802	3	0.300	40	15.814	2	0.277	14
69	-7.362	1	35.914	6	-7.364	2	36.028	10	-7.363	2	35.896	20
73.1	...	...	...	...	...	...	...	...	...	...	...	...
80.5	...	...	...	...	...	...	...	...	...	...	...	...
81.5	...	...	...	...	...	...	...	...	...	...	...	...

<sup>a</sup>In arcsec, errors ( $1\sigma$ ) are milli-arcsec.

<sup>b</sup>In km s<sup>-1</sup>, assuming  $D=450$  pc, relative to the reference feature, errors are  $1\sigma$ .

<sup>c</sup>Reference feature.

<sup>d</sup>UT days 312, 313.

<sup>e</sup>UT days 342, 343.

<sup>f</sup>UT day 59.

<sup>g</sup>UT day 156.

<sup>h</sup>UT day 321.

TABLE 1—Continued

1979 June <sup>a</sup>				1979 November <sup>b</sup>					Derived Proper Motions <sup>b</sup>		
$\Delta X$	$\sigma_{\Delta X}$	$\Delta Y$	$\sigma_{\Delta Y}$	$\Delta X$	$\sigma_{\Delta X}$	$\Delta Y$	$\sigma_{\Delta Y}$	$\Delta v_x$	$\sigma_{\Delta v_x}$	$\Delta v_y$	$\sigma_{\Delta v_y}$
-8.090	6	1.960	50	...	...	...	...	-64	13	...	...
...	...	...	...	-3.285	2	1.805	20	-7	13	...	...
-0.342	3	1.360	30	-0.348	2	1.371	20	-11	5	...	...
2.788	2	7.60	20	...	...	...	...	0	3	...	...
-3.728	1	3.723	2	-3.731	1	3.728	5	-19	2	48	10
...	...	...	...	...	...	...	...	...	...	...	...
-0.809	12	2.19	100	...	...	...	...	...	...	...	...
-3.449	6	1.83	60	...	...	...	...	...	...	...	...
-0.895	1	2.219	3	-0.895	2	2.20	20	-12	3	38	10
...	...	...	...	...	...	...	...	...	...	...	...
-0.581	4	2.105	30	-0.581	2	2.092	20	(0	20)	...	...
6.671	2	20.483	20	...	...	...	...	...	...	...	...
6.731	2	20.430	12	...	...	...	...	14	5	...	...
...	...	...	...	...	...	...	...	13	14	...	...
5.436	4	10.674	35	...	...	...	...	36	12	...	...
3.250	1	24.817	3	3.254	1	24.825	3	19	9	32	25
...	...	...	...	...	...	...	...	...	...	...	...
-3.789	1	-0.390	2	...	...	...	...	-5	3	-5	9
-3.099	1	-1.484	2	...	...	...	...	7	4	...	...
-3.297	2	1.893	25	-3.297	1	1.904	5	0	7	...	...
...	...	...	...	...	...	...	...	(0	30)	...	...
...	...	...	...	...	...	...	...	(-38	30)	...	...
-6.766	2	0.358	25	...	...	...	...	...	...	...	...
-0.144	2	0.265	20	...	...	...	...	-5	4	...	...
-9.249	2	1.810	40	-9.247	2	1.780	20	(6	14)	...	...
-7.704	2	-1.550	20	-7.707	3	-1.575	30	16	4	...	...
11.494	1	21.289	3	11.497	4	21.270	40	5	3	20	14
...	...	...	...	...	...	...	...	...	...	...	...
11.357	2	21.320	20	11.359	6	21.320	100	11	8	...	...
11.576	2	21.286	20	11.581	4	21.260	40	21	14	...	...
...	...	...	...	...	...	...	...	...	...	...	...
...	...	...	...	...	...	...	...	...	...	...	...
...	...	...	...	...	...	...	...	11	13	...	...
-8.664	3	-0.640	35	-8.675	2	-0.634	16	-36	4	...	...
...	...	...	...	...	...	...	...	-7	7	...	...
-8.691	2	-0.670	30	...	...	...	...	...	...	...	...
...	...	...	...	...	...	...	...	...	...	...	...
0	...	0	...	0	...	0	...	0	...	0	...
-3.579	1	-1.202	2	-3.584	1	-1.203	3	-23	8	-5	20
...	...	...	...	...	...	...	...	...	...	...	...
-0.065	1	0.090	2	-0.065	1	0.095	3	0	3	22	15
...	...	...	...	...	...	...	...	...	...	...	...
-0.110	2	0.119	30	-0.105	6	-0.050	120	...	...	...	...
-9.709	4	-1.09	50	-9.707	1	-1.106	8	-9	5	...	...
-7.368	4	-1.56	50	-7.404	6	-1.605	60	-54	17	...	...
0.262	1	-0.039	2	0.262	1	-0.040	5	-2	3	-1	10
...	...	...	...	-3.314	4	1.960	60	-13	8	...	...
...	...	...	...	...	...	...	...	(-24	50)	...	...
...	...	...	...	...	...	...	...	63	30	...	...
15.816	2	0.075	30	15.820	3	0.077	20	32	7	0	20
15.834	1	0.322	5	15.844	2	0.312	20	39	8	44	30
...	...	...	...	...	...	...	...	-9	13	...	...
-7.346	3	36.077	30	...	...	...	...	...	...	...	...
3.078	2	25.097	10	...	...	...	...	...	...	...	...
3.086	2	25.115	10	3.091	3	25.120	30	23	20	...	...

sky, can be written as

$$\Delta\Phi = -\omega\Delta\tau(\theta_X, \theta_Y) + [(\omega - \omega_{LB}) - (\omega' - \omega'_{LB})]\Delta\tau^C + (\omega - \omega')\Delta\tau^S + \Delta\Phi^{INS}, \quad (3)$$

where  $\Delta\Phi^{INS}$  is an instrumental phase term;  $\Delta\tau(\theta_X, \theta_Y)$  is the differential geometric time delay between signals from the two positions on the sky, which depends on the geometry of source and interferometer;  $\omega_{LB}$  and  $\omega'_{LB}$  are the sky frequencies of the lower band edges of the switch cycles in which the two features are located;  $\Delta\tau^C$  is the uncorrected time difference between the clocks at different stations; and  $\Delta\tau^S$  is the error in the geometric delay, caused by uncertainties in the baselines, source positions, and atmospheric propagation delay.

The fractional delay errors due to the frequency standard and atmosphere are about one part in  $10^{13}$ , which can cause phase shifts of about  $1^\circ$  over a 2 MHz band in 6 hours. This limits the positional accuracy to a few micro-arcsec. In practice, with the Mark II system at 22 GHz, this limit cannot easily be reached. The clock and baseline errors ( $\Delta\tau^C$ ,  $\Delta\tau^S$  in eq. [3]) usually dominate and can be measured to an accuracy of  $\sim 20$  ns by observations of compact extragalactic continuum sources. Unfortunately, apart from 3C 273, most of the detectable sources on long baselines at 1.3 cm (3C 345, 3C 84, and NRAO 150) are at high declinations. It is therefore difficult to estimate the  $z$ -components of the baselines (along the polar axis) to better than  $\sim 10$  m. The uncertainty in the  $z$ -components of the baselines is thus the dominant source of error in the delay calibration for the phase data of maser sources.

We think that the final delay calibration in our experiment is accurate to about 50 ns. This introduces a systematic slope of about  $20^\circ$ – $50^\circ$  of phase across the 2 MHz videoband and limits the positional accuracy to about 50 micro-arcsec.

As mentioned above, we switched between different sky frequencies to cover the velocity spread of  $\sim 100$  km s $^{-1}$  in maser sources. The local oscillators at different stations introduce a random phase shift between switch cycles. We did not have phase calibration instrumentation to correct for this phase shift. In the phase analysis, it was then necessary to solve for these constant instrumental phase offsets ( $\Delta\Phi^{INS}$  in eq. [3]) when comparing phases from different switch cycles.

Finally, in many cases the quality of phase positions is further degraded by source structure, that is, the blending of several features having the same velocity but different positions.

In practice, the analysis is as follows. The phase center is first shifted to a position close to that of the feature under investigation, as determined from a fringe rate analysis, and the data are averaged for a few minutes. The phase mapping program follows the slowly

changing residual phase by simple phase connection, recognizes a lobe shift on the first data point by including it in the instrumental term, and fits a relative position to the phase data over a track which is typically 8 hours long on one or more baselines.

#### d) Aperture Synthesis and Structure of Individual Masers

To overcome the problem of blending of maser features at the same velocity and to check for a complicated brightness distribution of individual masers, one can map the maser emission by aperture synthesis of data acquired on many baselines. An advantage of this method is that one can detect features that are about a factor of 5 weaker ( $\gtrsim 1$  Jy) than with fringe rate or phase analysis. The positional accuracy which can be achieved by aperture synthesis is comparable with that of phase analysis. In W51MAIN, the only source which we have synthesized so far, blending on scale sizes of 10–50 milli-arcsec ( $< a$  few  $10^{15}$  cm) is not severe, and all mapped maser features are compact spots of size  $< 1\text{--}3 \times 10^{13}$  cm (Paper II).

#### e) Resulting Positional Accuracies

Comparison of positions from fringe rates, phases, and aperture synthesis at the same and at different epochs leads to the following conclusions:

1. The accuracy of position estimates are limited by systematic effects, and formal statistical error estimates are usually low by at least a factor of 2. This has been taken into account in the errors adopted for the proper motions.

2. The accuracies of the *best fringe rate* positions are close to the values expected theoretically (0.1–0.2 milli-arcsec on long baselines; 1 milli-arcsec on short baselines).

3. Video-frequency dependent effects (caused by the uncertainties of baselines and clocks) and complications introduced by frequency switching make it difficult at present to measure positions by phase analysis or aperture synthesis to better than 50–100 micro-arcsec.

#### f) Determination of Distances from Proper Motions

It is possible to determine distances with VLBI techniques by comparing relative proper motions and radial velocities *within* a group of maser features. This method requires that both radial and proper motions are kinematic, and that the number of features with measured motions is large ( $N \gtrsim 20$ ). There are two limiting cases of the kinematics in which the method works best:

1. If the motions are predominantly random, as in a “turbulent” velocity field, one can compare the velocity

dispersion in the radial direction ( $\sigma_{v_r}$  [km s<sup>-1</sup>]) with that in the proper motion coordinates ( $\sigma_{\mu}$  [rad s<sup>-1</sup>]). If all velocity components are normally distributed with the same velocity dispersion, the distance  $D$  can be estimated from

$$D = \frac{\sigma_{v_r}}{\sigma_{\mu}}. \quad (4)$$

This is the method of *Statistical Parallax*, well known in stellar statistics (Trumpler and Weaver 1953). In order to find the true proper motion dispersion  $\sigma_{\mu}$  from the observed value  $\sigma_{\mu}^{\text{ob}}$ , one has to correct for the broadening of the observed dispersion by the finite measurement accuracy  $e_{\mu}$  of the proper motions with the formula

$$\sigma_{\mu}^2 = (\sigma_{\mu}^{\text{ob}})^2 - e_{\mu}^2. \quad (5)$$

Since the reference feature is also moving, its motion is included in the motions of all other features. This bias can be removed by calculating the dispersion about the mean or median motion. The systematic radial velocity of the source has a similar effect on the radial velocity data. Its value can be best estimated from high-resolution molecular line observations of the source. Both the mean proper motion and systematic radial velocity can usually be determined to a small fraction of the total velocity dispersion. Thus, the uncertainty in the observed velocity dispersion ( $\Delta\sigma/\sigma$ ) is not very sensitive to typical errors ( $\Delta v$ ) in the estimated mean:

$$\frac{\Delta\sigma}{\sigma} \sim \frac{1}{2} \left( \frac{\Delta v}{\sigma} \right)^2. \quad (6)$$

The accuracy to which distances can be estimated by this method is

$$\frac{\sigma_D}{D} \approx \left[ \frac{1}{4N} \left\{ \frac{2N}{M} + \left[ 1 - \left( \frac{e_{\mu}}{\sigma_{\mu}^{\text{ob}}} \right)^2 \right]^{-1} \right\} \right]^{\frac{1}{2}}, \quad (7)$$

where  $N$  is the number of maser features with measured transverse motions, and  $M$  is the number of features with measured radial velocities. Usually  $M$  is greater than  $N$ . If the proper motions are measured in both coordinates, the number of transverse velocity measurements is  $2N$ . Hence, with  $N=25$ ,  $M=50$ , and  $e_{\mu}/\sigma_{\mu}^{\text{ob}}=1/5$ , distances can be estimated to about 15%. We have successfully applied this method to the proper motion data from W51MAIN (Paper II) and W51NORTH (Paper III).

In reality, the radial and transverse velocity dispersions may not be equal or the velocity distributions may not be normal. Almost all radial velocities of masers in W51MAIN, for example, are redshifted with

respect to the velocity of the molecular cloud, or blueshifted in W51NORTH. This can lead to a biased estimate of the distance (see discussion in Papers II, III). Preferential beaming of the masers along or perpendicular to the direction of motion can also result in a biased estimate of the distance. Such a preferential beaming, however, would be easy to recognize in the observed shape of the spectrum of the H<sub>2</sub>O source. Beaming along the direction of motion would lead to a depression of the intensities near the systematic radial velocity, and beaming perpendicular to the direction of motion would result in a steep falloff of the intensities at the lowest and highest radial velocities. Neither of these is observed (Fig. 1) and, hence, there is no strong preferential beaming for the Orion-KL H<sub>2</sub>O masers.

2. Alternatively, if the kinematics are dominated by homogeneous streaming, such as expansion, one can model the three-dimensional structure of the source. In this *Expanding Cluster Parallax*, the observed proper motions, radial velocities, and the two coordinates on the sky are used along with the model to predict the third space coordinate and the transverse motions. The distance is then estimated by scaling the observed proper motions to the predicted transverse motions to reach an optimal solution in the least-squares sense. The accuracy of the estimated distances is in principle better than with the method of the *Statistical Parallax*, since the analysis is based on velocities rather than velocity dispersions. In reality, however, the uncertainty depends critically on the correlation of the distance with the model parameters and deviations from spherical expansion, and probably yields uncertainties similar to those of *Statistical Parallax*. We have applied the *Expanding Cluster Parallax* method to the proper motion data in Orion-KL.

### III. RESULTS

#### a) Proper Motion Data in Orion-KL

In Orion-KL there are strong, low velocity H<sub>2</sub>O features between  $V_{\text{LSR}} = -8$  and  $+28$  km s<sup>-1</sup> and, in addition, weaker high velocity features between  $-100$  and  $+85$  km s<sup>-1</sup> (Fig. 1). Table 1 is a list of relative positions of these masers and their proper motions between 1977 and 1979. The positions have been corrected for differential aberration, precession, and nutation across the map (a few milli-arcsec over 20") and are referenced to a common epoch (1977 November).

Figure 2 is a composite of the maps from all epochs. These maps were made with baselines from 800 to 3000 km (Haystack-NRAO, Onsala-MPI, MPI-Crimea, Onsala-Crimea) and do not show the large, resolved H<sub>2</sub>O "shell features" at  $V_{\text{LSR}} = -8$  to  $-4$  and  $13$  to  $18$  km s<sup>-1</sup> (stippled in Fig. 1) which are located within 1" of the compact infrared source IRC2 (Moran *et al.* 1977; Genzel *et al.* 1979b; Hansen 1980). The SiO maser

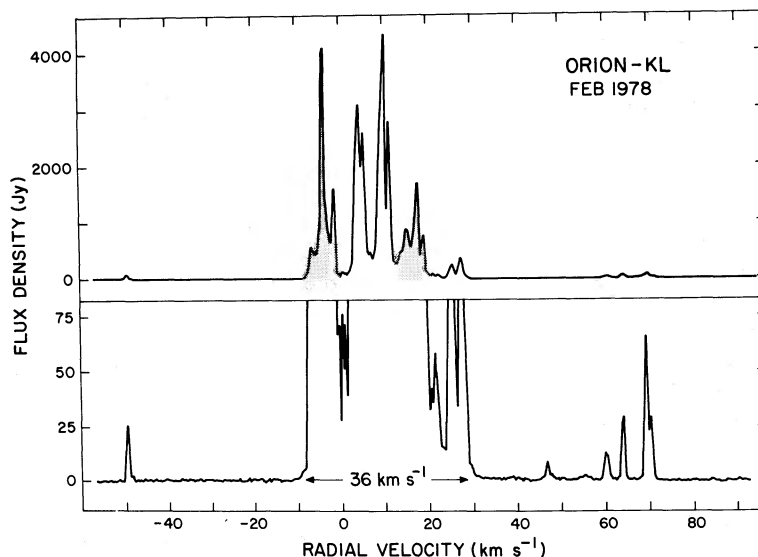


FIG. 1.—Total power spectrum of the 22 GHz  $\text{H}_2\text{O}$  maser emission in Orion-KL. The data were taken with the 100 m telescope on 1978 February 28. The spectral resolution is 32 kHz ( $0.43 \text{ km s}^{-1}$ ). The flux density scale is accurate to about  $\pm 30\%$ , and the radial velocities are with respect to the Local Standard of Rest and a rest frequency of 22 235.080 MHz. The stippled parts of the spectrum (upper) indicate the  $\text{H}_2\text{O}$  “shell features” which come from the immediate vicinity of the compact infrared source IRC2. The same spectrum is displayed truncated at the bottom, to emphasize the weak high velocity features. Not shown in this figure is a high velocity feature at  $-102 \text{ km s}^{-1}$ . The total velocity spread of the strong, low velocity lines is  $\sim 36 \text{ km s}^{-1}$ , around a mean of about  $10 \text{ km s}^{-1}$ . No attempt has been made to correct for gain variations over the antenna beamwidth.

source in Orion also originates from IRC2 (Genzel *et al.* 1979*b*; Baud *et al.* 1980). This is the only SiO maser found to date in a region of star formation. The  $\text{H}_2\text{O}$  masers in Orion-KL are grouped in “centers of activity” of size  $\sim 10^{16} \text{ cm}$  and are associated with several of the compact sources in the Kleinmann–Low Nebula. A detailed discussion of the relationship between masers and  $20 \mu\text{m}$  infrared emission, together with a description of the characteristics of IRC2 is given by Downes *et al.* (1981).

There are about 50 maser lines or tight spatial groups of maser features (multiple velocity knots) in this source. We have measured significant changes in the relative positions (of typically a few milli-arcsec per year) for more than 30 features. The data are displayed in Figure 3. Unfortunately, Orion is at low declination ( $-5^\circ$ ), and only a few motions in declination could be determined with the required accuracy. We interpret the positional changes shown in Figure 3 as kinematic motions of the maser spots for the following reasons. The derived proper motions (Table 1 and Fig. 3 for an assumed distance of 450 pc) are in accord with the radial velocities. The measured shifts in angle correspond to many times (5–50) the measured diameters of the masers and, hence, cannot simply be due to changes in the brightness distribution of individual maser spots. Furthermore, in the cases with the best positional accuracies, the position of the brightness maximum changes linearly with time as would be expected from motion at constant velocity. There may be a few cases, however,

where the apparent motion can be explained by variability of a complex brightness distribution (“Christmas Tree Effect”).

The proper motions of the masers in Orion show a large-scale trend when plotted against the angular offset from the reference feature (Fig. 4). Almost all the data points are in the first and third quadrants of this plot and form a tight crossing through the origin. From Figure 4 we conclude that all low velocity masers and possibly the high velocity masers (filled dots in Fig. 4) are *expanding away* from a *common central source*. If we assume that the expansion velocity depends only on the distance,  $R$ , from the center of expansion and follows a power law with exponent  $\alpha$ , the transverse velocity  $v_x$  as function of offset  $x$  in right ascension from the center of expansion will be

$$v_x(x) = v_e R^\alpha (x/R), \quad (8)$$

where  $v_e$  is the expansion velocity at a radius of  $R=1''$ . An analogous equation holds for the  $y$ -motions in declination. If the masers were confined to an expanding, thin shell of radius  $R$ , all data points in a plot of  $v_x$  versus  $x$  or  $v_y$  versus  $y$  would lie on a straight line with positive slope and zero intercept. In an expanding, thick shell, all data points would lie between two lines of different slopes. For constant expansion ( $\alpha=0$ ), the slope is inversely proportional to radius, so the outer and inner radii of the shell are represented by the smallest and greatest slopes, respectively. For a *con-*

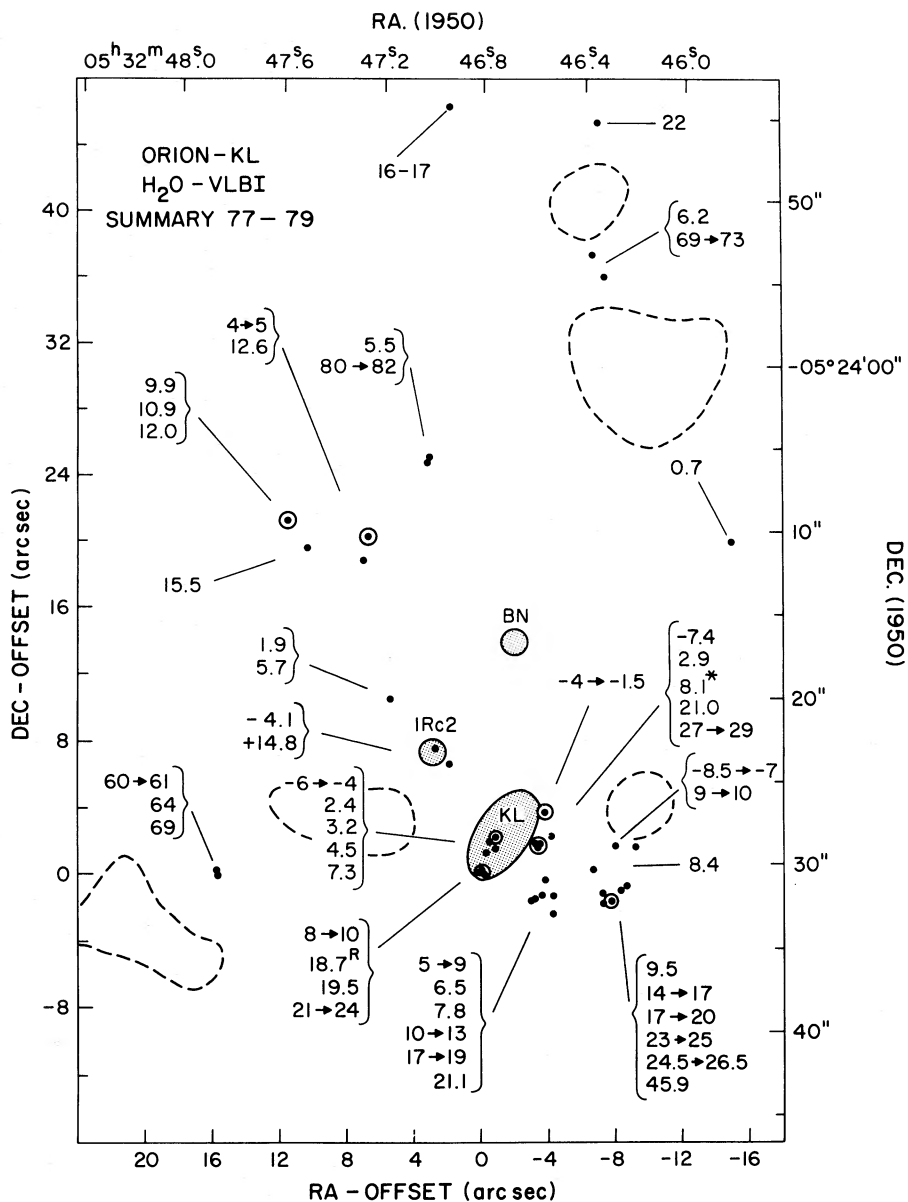


FIG. 2.—Spatial distributions of  $\text{H}_2\text{O}$  masers in Orion-KL, relative to the feature at  $V_{\text{LSR}} = 18.7 \text{ km s}^{-1}$ . The map is a composite of VLBI maps made between 1977 and 1979 (Table 1). Dots indicate individual maser features or groups of maser features; encircled dots indicate strong ( $\geq 4000 \text{ Jy}$ ), stable low velocity  $\text{H}_2\text{O}$  features. Labels are LSR velocities in  $\text{km s}^{-1}$ . The  $\text{H}_2\text{O}$  “flare” maser ( $\geq 10^6 \text{ Jy}$ , Abraham, Opher, and Raffaelli 1979) at  $8.1 \text{ km s}^{-1}$  is indicated by an asterisk. The absolute position of the reference feature is:  $05^{\text{h}}32^{\text{m}}46^{\text{s}}.82 \pm 0^{\text{s}}.02$ ,  $-05^{\circ}24'30''.6 \pm 0''.5$  (1950) derived from Forster *et al.* (1978). The stippled regions indicate the positions of compact near-infrared sources (Rieke, Low, and Kleinmann 1973; Wynn-Williams and Becklin 1974). BN is the Becklin-Neugebauer object, and KL is the core of the extended  $20 \mu\text{m}$  Kleinmann-Low Nebula. The  $\text{H}_2\text{O}$  maps have been derived from baselines longer than 800 km and do not show the large  $\text{H}_2\text{O}$  maser “shell features” which coincide with the compact infrared source IRC2 (Hansen 1980). IRC2 is also the location of the SiO maser in Orion (Baud *et al.* 1980), and most of the 1665 MHz OH masers arise within a few arcsec of IRC2 (Norris, Booth, and McLaughlin 1980; Hansen, private communication). The dashed lines indicate the peaks of  $2 \mu\text{m}$  quadrupole line emission from molecular hydrogen (Beckwith *et al.* 1978). At a distance of  $\sim 480 \text{ pc}$ ,  $10''$  corresponds to  $7.2 \times 10^{16} \text{ cm}$ .

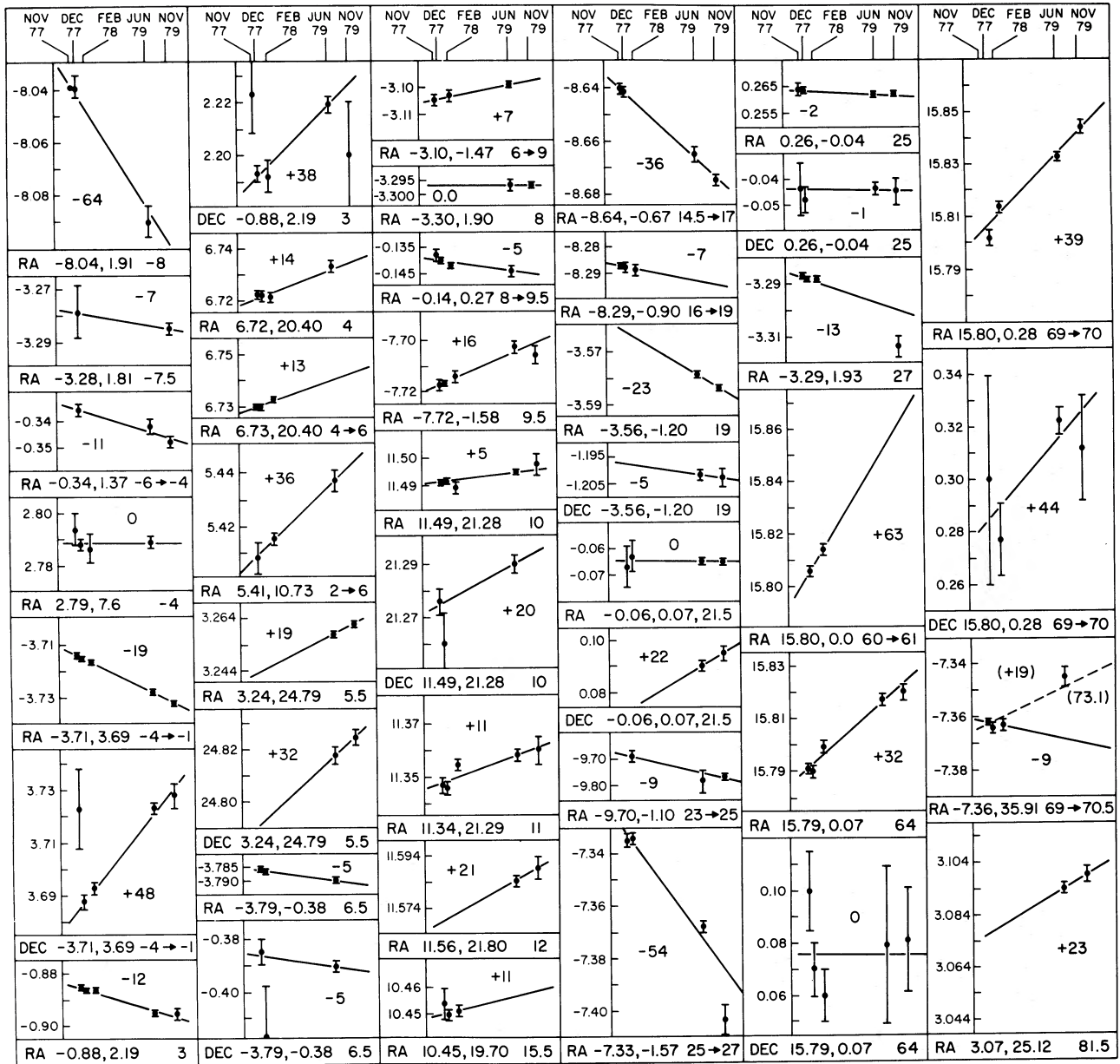


FIG. 3.—Proper motions of H<sub>2</sub>O maser features in Orion-KL. The positions of H<sub>2</sub>O maser features are shown separately for R.A. and decl. (if available) as a function of time, relative to the reference feature at  $V_{\text{LSR}} = 18.7 \text{ km s}^{-1}$ . The UT day numbers of the experiments (indicated at the top) are as follows: 312–313 (1977 November), 342–343 (1977 December), 59 (1978 February), 156 (1979 June), and 321 (1979 November). The angular scale (vertical axis) is in units of arcsec. Error bars on the positions are  $1\sigma$ . The straight lines are weighted least-squares which yield the indicated proper motion velocities ( $\text{km s}^{-1}$  for an assumed distance of 450 pc). The boxes below each diagram give (from left to right): proper motion coordinate (R.A. or decl. motion), the approximate relative position in arcsec (R.A., decl.), and the radial velocity of the maser feature in  $\text{km s}^{-1}$ . Multiple velocity knots with the same proper motion are given as one feature.

tracting source, on the other hand, all data points would lie in the second and fourth quadrants between two lines of negative slope. Finally, in a rotating source, the data points would fall in all four quadrants between two concentric ellipses. Figure 4, therefore, shows that the low velocity features are expanding at  $\sim 20 \text{ km s}^{-1}$  and come from a region of inner radius  $\sim 1''$  and outer radius  $\sim 25''$ .

In reality, one does not measure the true transverse motion  $v_x$  given in equation (8), but a “referenced” velocity  $\Delta v_x$ , given by

$$\Delta v_x(x) = v_e R^\alpha \left( \frac{x}{R} \right) - v_e R_0^\alpha \left( \frac{x_0}{R_0} \right), \quad (9)$$

where  $R_0$  and  $x_0$  are the radius and  $x$ -coordinate of the

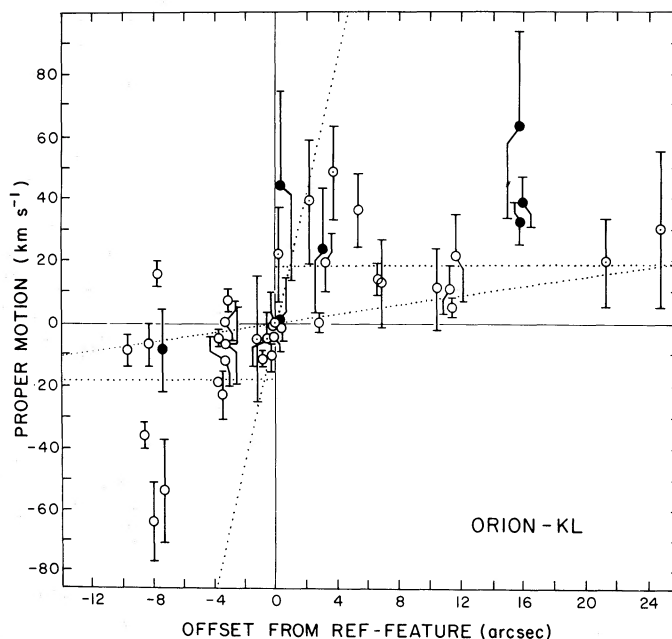


FIG. 4.—Relative proper motions ( $\text{km s}^{-1}$ , for a distance of 450 pc) of H<sub>2</sub>O maser features in Orion-KL, plotted against the angular offset from the reference feature (in arcsec, where  $10''$  corresponds to  $\sim 7 \times 10^{16}$  cm). Open circles are R.A.-motions, open circles with a dot are decl.-motions, and filled circles are high velocity features ( $|V_{\text{LSR}} - 10 \text{ km s}^{-1}| > 20 \text{ km s}^{-1}$ ). Error bars are  $1\sigma$ . As described in § III a, the data show a large scale outflow of material from a central source. The dotted lines indicate the expansion velocity of most low velocity features ( $18 \text{ km s}^{-1}$ , horizontal lines), the innermost shell of the expanding source (radius  $\sim 1''$ , steeper slope) and the outermost shell (radius  $\sim 25''$ , shallow slope). The three open circles at offset  $\sim -8''$  and proper motion velocities  $-35$  to  $-65 \text{ km s}^{-1}$  probably are high velocity features with a low projected radial velocity.

reference feature with respect to the center of expansion, respectively. An analogous equation holds for the  $y$ -motions. The tight crossing through the origin in Figure 4 (R.A. motions) indicates that the  $x$ -coordinate of the reference feature must lie near the center of expansion and that there cannot be several centers of expansion separated by more than a few seconds of arc.

Figure 5 is a plot of the radial velocities (with respect to  $V_{\text{LSR}} = 10 \text{ km s}^{-1}$ ) versus the angular distance between maser feature and reference position. In this diagram, data points from an expanding, thin shell would fall on an ellipse whose intercept with the radial velocity axis gives the value of the expansion velocity, while the  $x$ -axis intercept gives the radius of the shell. As with the proper motions, the radial motions of the low velocity masers are as expected for an expanding, thick shell. The thin ellipse represents the outermost boundary of radius  $\sim 25''$  and expansion velocity  $\sim 18 \text{ km s}^{-1}$  (see also the velocity spread of the low velocity emission in Fig. 1). The black dots in Figure 5 denote the high velocity masers; their kinematics are different from those of the low velocity features and cannot be explained by a uniform outflow of material at constant expansion velocity. Thus, the proper motion and radial velocity data of the H<sub>2</sub>O masers indicate that there are two distinct outflows in the Orion-KL region.

#### b) Model of the Orion-KL Outflow

We have fit the proper motion and radial velocity data with a model of a radially expanding source, using the observed relative maser positions on the sky ( $x, y$ ) and the three dimensional space velocities ( $\Delta v_x, \Delta v_y$ , if available, and  $v_z$ ). The space velocities were treated as observables in equation (9), and a weighted least-squares solution was calculated for  $v_e, \alpha$ , the origin of the expansion ( $x_0, y_0, z_0$ ), the distance of the source ( $D$ ), and the  $z$ -coordinates (along the line of sight) of all features. The least-squares problem is nonlinear, and we investigated a wide range of the parameters in order to find the best solution. Most parameters were not highly correlated, and the solutions were unambiguous. The results are summarized in Table 2. The main conclusions are as follows.

##### i) Low Velocity Flow ( $18 \text{ km s}^{-1}$ )

1. The expansion velocity of the low velocity flow is  $18 \pm 2 \text{ km s}^{-1}$ , and constant from  $1''$  to  $22''$  in radius ( $\alpha = 0 \pm 0.1$ ).

2. The best estimate of the center of the expansion [ $05^{\text{h}} 32^{\text{m}} 46^{\text{s}}.8 \pm 0^{\text{s}}.1, -05^{\circ} 24' 27'' \pm 2''$  (1950)] lies between the core of the KL (IRc4, Rieke, Low, and Kleinmann 1973; Wynn-Williams and Becklin 1974; Downes *et al.* 1981) and IRc2 (Fig. 6). The BN object

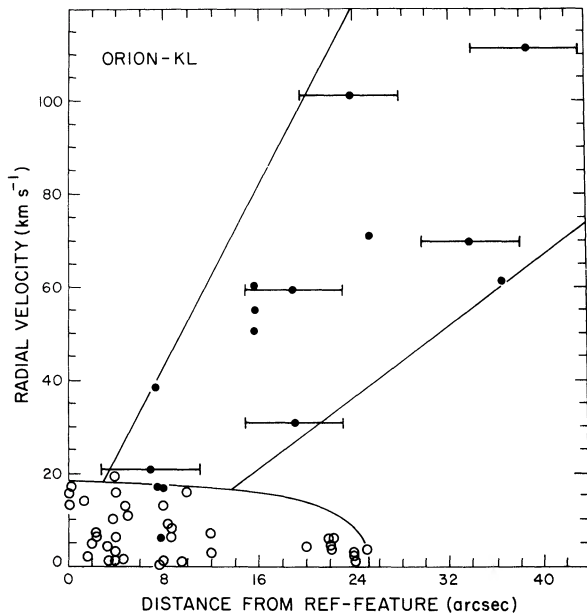


FIG. 5.—Radial velocities ( $|V_{\text{LSR}} - 10 \text{ km s}^{-1}|$ ) of  $\text{H}_2\text{O}$  masers in Orion-KL, plotted against the angular distance from the reference feature (in arcsec, where  $10''$  corresponds to  $\sim 7 \times 10^{16}$  cm). Shown are all masers listed in Table 2, as well as several high velocity masers measured with the 100 m telescope (large error bars, Downes and Genzel 1980). Open circles are low velocity  $\text{H}_2\text{O}$  masers; filled circles are high velocity masers. The thin ellipse represents an expanding shell of radius  $25''$  and expansion velocity  $18 \text{ km s}^{-1}$ .

cannot be the center of the “ $18 \text{ km s}^{-1}$ ” flow. IRC2 is inside the  $2\sigma$  error box and the spatial distribution of the low velocity masers is roughly centered on it. Because of this agreement and, in particular, because the expansion velocity of  $18 \text{ km s}^{-1}$  for the low velocity flow is identical with the value determined from the SiO/ $\text{H}_2\text{O}$  “shell features” in the immediate vicinity of IRC2 (Genzel *et al.* 1980), we will henceforth assume that the low velocity  $\text{H}_2\text{O}$  flow is associated with IRC2.

3. The LSR velocity centroid of the  $18 \text{ km s}^{-1}$  flow is  $10 \text{ km s}^{-1}$ . This is offset from  $5.5 \text{ km s}^{-1}$ , the centroid of the SiO/ $\text{H}_2\text{O}$  “shell features” which may be the LSR velocity of IRC2 itself. This discrepancy is easily seen in the  $\text{H}_2\text{O}$  spectrum in Figure 1 and is probably significant. The low velocity masers in Orion are usually very stable and a velocity centroid of  $\sim 10 \text{ km s}^{-1}$  is consistent with all  $\text{H}_2\text{O}$  spectra taken over the past 10 years (Sullivan 1973; Hansen 1980). On the other hand, the velocity centroid of  $10 \text{ km s}^{-1}$  is close to the LSR velocity of the quiescent molecular cloud ( $\sim 9 \text{ km s}^{-1}$ ). This may indicate an interaction between the outflow and the dense surrounding cloud.

If IRC2 had a transverse velocity vector  $\Delta v$  with respect to the surrounding cloud, the apparent center of expansion of the flow at radius  $R$  would be different from the current position of IRC2 by  $\Delta R$ :

$$\Delta R \approx -\frac{R}{v_e} \Delta v. \quad (10)$$

Let us assume  $v_e = 18 \text{ km s}^{-1}$ ,  $R = 10'' - 20''$ , and  $\Delta v \sim 4 \text{ km s}^{-1}$  which is comparable to the offset in radial velocity. The apparent center of the expansion would then be displaced from the current position of IRC2 by a few arcsec, in agreement with the observations, and the velocity vector of IRC2 would point out of the KL nebula.

4. The  $x$ - $y$  distribution of the masers on the sky is nonrandom and clumpy. Most of the masers are found in a NE-SW strip stretching about  $10''$  on both sides of IRC2. There is a clear enhancement in the projected density of masers where the flow seems to encounter the infrared condensations in the KL Nebula. A comparison with the  $x$ - $z$  distribution indicates that most of these “centers of activity” projected onto the  $x$ - $y$  plane are probably true *three-dimensional* clumps. These clumps are very similar to the compact features observed on high-resolution  $20 \mu\text{m}$  maps (e.g., IRC3, IRC4, etc., Downes *et al.* 1981).

5. We estimate the distance to Orion-KL to be  $480 \pm 80$  pc. This value is at least as accurate as the optical determinations from statistical parallaxes and stellar luminosities which range from 380 to 520 pc (e.g., Markowitz 1949; Parenago 1954; Johnson and Hiltner 1956; Strand 1958; Johnson 1965). The formal uncertainty ( $1\sigma$ ) in the estimate of the distance is  $\pm 50$  pc. We have studied the sensitivity of the distance parameter to changes in the model and estimate that systematic errors can change the distance by up to  $\pm 60$  pc. Hence, our total error is  $\pm 80$  pc.

#### ii) High Velocity Flow ( $30\text{--}100 \text{ km s}^{-1}$ )

1. To within the errors of about  $5''$ , the best estimate for the center of expansion of the high velocity flow agrees with that of the low velocity flow. The  $2\sigma$  error box for the centroid of the high velocity flow includes IRC2, but also BN and most of the other compact infrared sources in the Orion-KL region. The high velocity zone is larger than the  $18 \text{ km s}^{-1}$  zone by about a factor of 1.5–2 and exhibits a positive velocity exponent ( $\alpha = 0.3 \pm 0.1$ ).

2) Inspection of the  $x$ - $y$  and  $x$ - $z$  planes indicates that the most prominent and stable high velocity features are far from IRC2, in the NW and SE corners of the map. A few high velocity masers are, however, close to masers in the low velocity flow.

#### IV. CHARACTERISTICS OF THE OUTFLOW

##### a) The $\text{H}_2\text{O}$ Outflow Is the Same Phenomenon as the Molecular “Plateau” Emission

We have presented evidence that there are two different, large-scale outflows of  $\text{H}_2\text{O}$  maser cloudlets in the Orion-KL region. The  $18 \text{ km s}^{-1}$  flow seen in the  $\text{H}_2\text{O}$  and SiO maser emission can be attributed to the compact infrared source IRC2. The 1665 MHz maser emission of OH and the  $v=0, J=1-0$  “thermal” emis-

TABLE 2  
PARAMETERS OF THE H<sub>2</sub>O OUTFLOW IN ORION

Parameter	Low Velocity Flow <sup>a</sup> (“18 km s <sup>-1</sup> ” Flow)	High Velocity Flow <sup>a</sup> (30–100 km s <sup>-1</sup> )
Expansion Velocity, $v_e$ (km s <sup>-1</sup> ) at $R=1''$ .....	18 ± 2	24 ± 8
Exponent of Velocity Law, $\alpha$ ( $v=v_e R^\alpha$ ) .....	0.0 ± 0.1	0.3 ± 0.1
Origin of Expansion with Respect to Reference Feature <sup>b</sup> , (arcsec)		
$x_0$ .....	0 <sup>o</sup> .2 ± 1 <sup>o</sup> .0 <sup>cd</sup>	0 <sup>o</sup> .0 ± 2 <sup>o</sup> .0 <sup>d</sup>
$y_0$ .....	3 <sup>o</sup> .5 ± 2 <sup>o</sup> .0	4 <sup>o</sup> .5 ± 6 <sup>o</sup> .0
$z_0$ .....	2 <sup>o</sup> .0 { + 3 <sup>o</sup> .0 - 1 <sup>o</sup> .5	...
Radial (LSR) Velocity Centroid of Outflow, $U_0$ (km s <sup>-1</sup> ) .....	10 ± 2	...
Minimum Radius $R_{\text{MIN}}$ (arcsec) .....	1 <sup>o</sup> .5 ± 0 <sup>o</sup> .5 <sup>d</sup>	6 <sup>o</sup> ± 4 <sup>o</sup> . <sup>d</sup>
Maximum Radius $R_{\text{MAX}}$ (arcsec) .....	22 <sup>o</sup> ± 3 <sup>o</sup>	50 <sup>o</sup> { + 100 <sup>o</sup> - 20 <sup>o</sup>
Distance (pc) .....	480 ± 80	...

<sup>a</sup>Error bars are  $1\sigma$ .

<sup>b</sup> $x_0$  is true angle, increasing toward East;  $y_0$  is increasing North;  $z_0$  is increasing away from the observer; the absolute position of the reference feature is: 05<sup>h</sup>32<sup>m</sup>46<sup>s</sup>.82, -05<sup>o</sup>24<sup>'</sup>30<sup>o</sup>.6 (1950).

<sup>c</sup>For comparison, IRC2 has:  $x_0 = 2<sup>o</sup>.8$ ,  $y_0 = 7<sup>o</sup>.6$ ; BN has  $x_0 = -1<sup>o</sup>.9$ ,  $y_0 = 14<sup>o</sup>.0$ .

<sup>d</sup>At 480 pc, 1<sup>o</sup> corresponds to  $7.2 \times 10^{15}$  cm.

sion of SiO also come from IRC2 (Norris, Booth, and McLaughlin 1980; Hansen, private communication; Genzel *et al.* 1980; Baud *et al.* 1980). Though less well defined than the thermal SiO, the position of the “plateau” emission of NH<sub>3</sub> and HCN is definitely south of BN (Wilson, Downes, and Bieging 1979; Rydbeck *et al.* 1980), and is consistent with outflow from IRC2. We therefore suggest that *all* molecular “plateau” sources with a total velocity spread of about 40 km s<sup>-1</sup> originate from that source.

Figure 7 is a composite from several published measurements of velocities of molecular lines in the Orion-KL region. The 18 km s<sup>-1</sup> flow reaches terminal velocity at a few  $10^{14}$  cm and can be followed in several “plateau” lines out to a radius of about 30<sup>o</sup> ( $2 \times 10^{17}$  cm). It is remarkable that the outflow velocity stays constant at 18 km s<sup>-1</sup> over 3 orders of magnitude in radius. This implies that the outflow is *steady* and *continuous* with a duration of  $\gtrsim 3000$  years. An explosive event with a differentially expanding envelope (e.g., Kwan and Scoville 1976) is unlikely.

The “plateau” profiles of the 2  $\mu$ m quadrupole transitions of H<sub>2</sub> (Nadeau and Geballe 1979, 1980), and of the 115 GHz  $J=1-0$  transition of CO (after subtraction of the “spike”-component; Zuckerman, Kuiper,

and Rodriguez-Kuiper 1976; Kwan and Scoville 1976; Kuiper, Rodriguez-Kuiper, and Zuckerman 1978) can be separated into a central part of full width at zero power 40 km s<sup>-1</sup> (that is,  $\pm 20$  km s<sup>-1</sup>) and broad outer wings out to  $\pm 80$  km s<sup>-1</sup> in radial velocity. We believe that these two components correspond, respectively, to the 18 km s<sup>-1</sup> and the high velocity flows found in the H<sub>2</sub>O maser emission.

#### b) Interaction with the Surrounding Molecular Cloud: The Hot Gas

The outflow probably has a large influence on the surrounding dense molecular cloud and vice versa. The nonmetastable lines of ammonia (Morris, Palmer, and Zuckerman 1980; Zuckerman, Palmer, and Morris 1980) and the methanol masers (Matsakis *et al.* 1980), for example, suggest that there are dense clumps of hot ( $T_k > 100$  K), quiescent ( $\Delta v \lesssim 6$  km s<sup>-1</sup>) gas, either embedded in or just outside of the outflow (Fig. 7). Further support for this picture comes from the extent and clumpy structure of the 20  $\mu$ m infrared emission. The size of the extended 20  $\mu$ m nebula is similar to that of the 18 km s<sup>-1</sup> flow, and there is good correlation between clumps of 20  $\mu$ m emission and “centers of

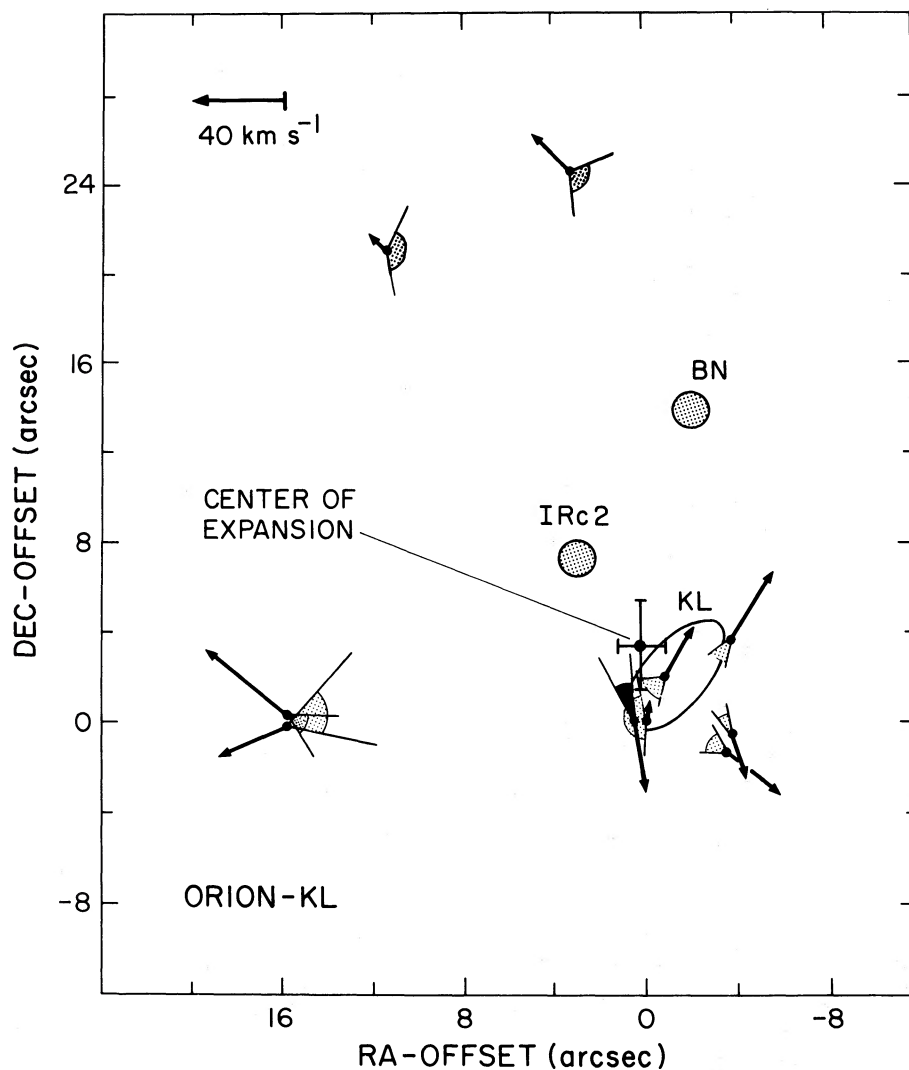


FIG. 6.—Two-dimensional proper motions and the center of expansion in Orion-KL. Shown are all proper motion vectors (for the cases with decl.-motions) with length proportional to their transverse velocity, and error bars ( $1\sigma$ ) indicated by error cones (stippled). The best estimate for the center of the  $18 \text{ km s}^{-1}$  flow from the model described in the text is shown with  $1\sigma$  error bars (position:  $05^{\text{h}}32^{\text{m}}46^{\text{s}}8 \pm 0^{\text{s}}1$ ,  $-05^{\circ}24'27'' \pm 2''$ ) (1950). For comparison, positions of some of the infrared features in Orion-KL also are indicated (stippled regions). BN is the Becklin-Neugebauer object, KL is the core of the extended  $20 \mu\text{m}$  Kleinmann-Low Nebula. The compact infrared source IRc2 is the location of the SiO maser in Orion. All velocity vectors are relative to the center of expansion, that is, they have been corrected for the motion of the reference feature from the model parameters.

$\text{H}_2\text{O}$  maser activity" in the flow (see discussion in Downes *et al.* 1981). A lower limit to the mass of this dense, hot gas is about  $10 M_{\odot}$ .

c) *Can Radiation Pressure Drive the Outflow?*

The mass loss in the  $18 \text{ km s}^{-1}$  flow,  $\dot{M}_{lv}$ , can be estimated from thermal molecular lines if the source size and excitation temperature are known and if the emission is moderately optically thin. We estimate an average value from the  $v=0$  lines of SiO (after allowing for 50–90% depletion of gaseous Si onto grains) and

the CO rotational transitions following the derivation of Morris (1975) and Genzel *et al.* (1980) to be

$$\dot{M}_{lv} = 10^{-3 \pm 1} M_{\odot} \text{yr}^{-1}. \quad (11)$$

The momentum transport and mechanical luminosity carried by this low velocity (lv) flow are given by

$$(\dot{M}v)_{lv} = 10^{29 \pm 1} \text{ergs cm}^{-1}, \quad (12)$$

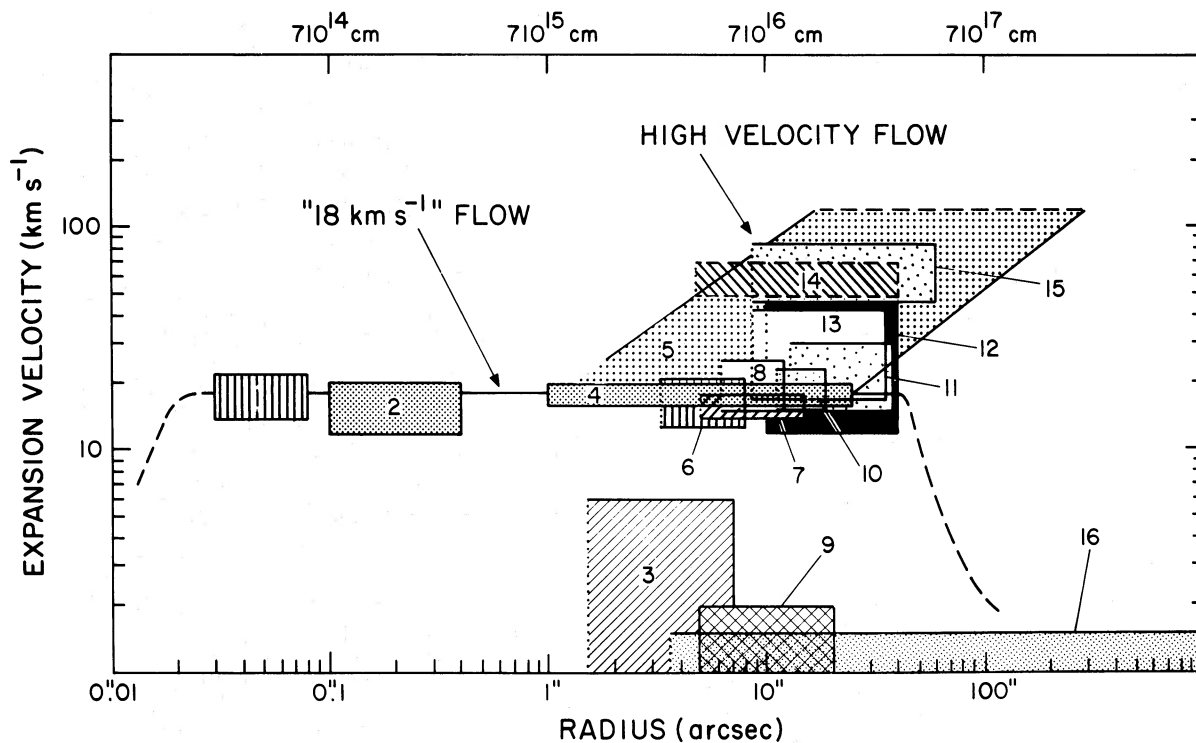


FIG. 7.— Expanding flows in the Orion-KL region. Plotted on a logarithmic scale are estimates for the expansion velocity ( $\text{km s}^{-1}$ ) vs. projected radius from IRC2 (arcsec, with the linear scale indicated at the top) from published observations of molecular lines. Boxes give uncertainties or ranges for the velocities and sizes of the molecular line sources. A dotted left margin of a box indicates that there is only an upper limit for the inner radius of the source. Numbers indicate the following observations: (1) vibrationally excited SiO maser “shell features” (43 GHz, Genzel *et al.* 1979b); (2) H<sub>2</sub>O maser “shell features” (22 GHz, Hansen 1980); (3) nonmetastable ammonia “hot core” (21–25 GHz, Morris, Palmer, and Zuckerman 1980); (4) H<sub>2</sub>O 18  $\text{km s}^{-1}$  flow (23 GHz, this paper); (5) H<sub>2</sub>O high velocity flow (this paper); (6) ground vibrational “thermal” SiO (43, 86 GHz, Genzel *et al.* 1980; Baud *et al.* 1980); (7) ammonia “plateau” (23 GHz, Wilson, Downes, and Bieging 1979); (8) SO<sub>2</sub> “plateau” (250 GHz, Wannier *et al.* 1980); (9) methanol maser features (25 GHz, Matsakis *et al.* 1980); (10)  $J=3-2$  CO “plateau” (345 GHz, Phillips *et al.* 1977); (11)  $J=2-1$  CO “plateau” (230 GHz, Wannier and Phillips 1977; Wannier *et al.* 1980); (12)  $J=1-0$  CO “plateau” (inner wings) (115 GHz, Zuckerman, Kuiper, Rodriguez-Kuiper 1976; Kwan and Scoville 1976; Kuiper, Rodriguez-Kuiper, and Zuckerman 1978; Scoville 1980); (13) S(1) H<sub>2</sub> quadrupole emission (central part) (2  $\mu\text{m}$ , Nadeau and Geballe 1979, 1980); (14) S(1) H<sub>2</sub> quadrupole emission (wings) (2  $\mu\text{m}$ ); (15)  $J=1-0$  CO “plateau” (outer wings) (115 GHz); (16)  $J=1-0$  “spike” (115 GHz, Liszt *et al.* 1974). The dashed lines indicate where the 18  $\text{km s}^{-1}$  flow may reach terminal velocity and where it might be stopped in the surrounding molecular cloud.

and

$$(\dot{M}v^2/2)_{\text{iv}} = 10^{1.5 \pm 1} L_{\odot}.$$

The high velocity wings in the  $J=1-0$  profile of CO are an appreciable part of the integrated intensity of the whole “plateau” feature. The mass loss in the high velocity wings must therefore be about 5–50% of the mass loss in the low velocity flow, if the emission is optically thin ( $\dot{M}_{\text{hv}} \approx 10^{-4 \pm 1} M_{\odot} \text{ yr}^{-1}$ ). The total momentum transport in the high velocity (hv) flow may therefore be comparable with that in the 18  $\text{km s}^{-1}$  flow:

$$(\dot{M}v)_{\text{hv}} \sim (\dot{M}v)_{\text{iv}}. \quad (13)$$

This rough “equipartition” implies that the mechanical luminosity of the high velocity flow is  $> 10^2 L_{\odot}$ , that is, greater than that of the 18  $\text{km s}^{-1}$  flow. This may be

enough to account for the luminosity ( $\sim 10^{3 \pm 1} L_{\odot}$ ) estimated for the H<sub>2</sub> quadrupole line emission at 2  $\mu\text{m}$  (Beckwith *et al.* 1978).

The mass loss phenomena in Orion-KL probably cannot be driven by radiation pressure alone. The deep 9.7  $\mu\text{m}$  silicate feature in the spectrum of IRC2 indicates  $L_{\text{IRC2}} > 10^4 L_{\odot}$  (Downes *et al.* 1981) and may even be close to  $10^5 L_{\odot}$ , which is a large fraction of the total far-infrared luminosity of the entire Orion-KL region (Werner *et al.* 1976). But even if the luminosity of IRC2 were close to this upper limit and radiation pressure were efficiently transferred to the outflow ( $\epsilon_{\text{rad}} \gtrsim 0.5$ ), as in late-type giants and supergiants, the momentum transport available from radiation would be at most

$$\epsilon_{\text{rad}} \frac{L_{\text{IRC2}}}{c} < 10^{28} \text{ ergs cm}^{-1}. \quad (14)$$

Since this is probably an extreme upper limit, we feel that it is unlikely that radiation pressure alone could account for the  $\sim 10^{29}$  ergs  $\text{cm}^{-1}$  observed in the outflows (see the discussions in Zuckerman, Kuiper, and Rodriguez-Kuiper *et al.* 1976; Kwan and Scoville 1976; Beckwith *et al.* 1978).

Therefore, we think that the large mass loss is more likely driven by the loss of rotational, magnetic, or gravitational energy from IRC2. Possible mechanisms are hydrodynamic instabilities in the envelope of a rapidly rotating young star (Larson 1980), wind driven turbulence in a circumstellar disk (Elmegreen 1978), pulsational instabilities in the envelope of a star (Hoyle, Solomon, and Woolf 1973), and transport of angular momentum by magnetic fields (Lüst and Schlüter 1955; Ebert, von Hoerner, and Tómesvary 1960).

#### d) Why Are There Two Types of Outflow?

We now discuss possible explanations for the two types of outflow in Orion-KL.

1. There are two different central sources, each producing its own outflow. For example, BN may cause the high velocity flow while IRC2 produces the low velocity flow. The  $2\sigma$  error box for the center of the high velocity  $\text{H}_2\text{O}$  flow includes the BN object; and high-resolution observations of the  $\text{B}\alpha$  hydrogen recombination line at  $4\ \mu\text{m}$  toward BN (Hall *et al.* 1978; Scoville 1981) indicate broad wings over  $\sim 100\ \text{km s}^{-1}$ . There are two arguments against this picture. First, several other  $\text{H}_2\text{O}$  sources in regions of star formation (e.g., W51MAIN, W49N, W3OH) also show a core of low velocity  $\text{H}_2\text{O}$  lines surrounded by  $\text{H}_2\text{O}$  high velocity emission. It seems unlikely that in all of these cases two objects are simultaneously undergoing mass loss with a dynamical time scale of  $10^3$ – $10^4$  yr. Second, the observations of near-infrared hydrogen recombination lines show that there is a small HII region around BN. The  $\text{B}\alpha$  flux corresponds to a total number of Lyman continuum photons  $N_{\text{Lyc}}$  of a few times  $10^{46}\ \text{s}^{-1}$  (Hall *et al.* 1978). If BN were the source of the high velocity outflow ( $> 10^{-5} M_{\odot}\ \text{yr}^{-1}$ ), it probably would have no measurable HII region for the following reason: In a wind with density proportional to  $R^{-2}$ , the critical mass loss required to suppress the formation of an HII region is given by

$$\left[ \frac{\dot{M}_{\text{crit}}}{M_{\odot}\ \text{yr}^{-1}} \right] = 4 \times 10^{-7} \left[ \frac{v_w}{100\ \text{km s}^{-1}} \right] \times \left[ \frac{N_{\text{Lyc}}}{10^{46}\ \text{s}^{-1}} \right]^{\frac{1}{2}} \left[ \frac{R_F}{10^{12}\ \text{cm}} \right]^{\frac{1}{2}} \quad (15)$$

(e.g., Wright and Barlow 1975), where  $R_F$  is the radius of the origin of the flow (see discussion in Downes *et*

*al.* 1981). Thus, the mass loss rate of the high velocity flow may be sufficient to inhibit the formation of an HII region.

2. The rate and outflow velocity of the mass loss are time variable. One would indeed expect a good deal of variability from the possible mass loss mechanisms mentioned above. However, our model of the  $18\ \text{km s}^{-1}$  flow indicates a smooth, continuous outflow at constant expansion velocity over the past  $10^3$ – $10^4$  years. Furthermore, the observations of low and high velocity masers in most strong  $\text{H}_2\text{O}$  sources in the Galaxy strongly suggest that these two types of masers occur simultaneously, or that flares and variability occur on short time scales ( $\ll 10^3$  yr).

3. Both the low velocity and high velocity flows are driven by a fast ( $v_w > 100\ \text{km s}^{-1}$ ) stellar wind from IRC2. If the dense cloud around IRC2 is clumpy and nonspherically distributed, bits and pieces of the wind could escape along paths of the largest density gradients and accelerate dense cloudlets of gas to velocities of  $30$ – $100\ \text{km s}^{-1}$  which are observed as high velocity  $\text{H}_2\text{O}$  masers. This hypothesis may be supported by the spatial distribution of the masers. The material in the  $18\ \text{km s}^{-1}$  flow of the  $\text{H}_2\text{O}$  and OH masers (this paper; Norris, Booth, and McLaughlin 1980; Hansen, private communication) does lie preferentially in a NE-SW strip around IRC2, whereas the most stable high velocity features are NW-SE from the center. Furthermore, the spatial distribution of the  $2\ \mu\text{m}$   $\text{H}_2$  quadrupole lines (Beckwith *et al.* 1978) also peaks in the NW-SE directions from IRC2. This morphology may indicate an enhanced density of high velocity  $\text{H}_2$  gas in these directions or possibly a large extinction in the dense gas of the low velocity flow between the  $\text{H}_2$  peaks. Both cases would be consistent with the picture given above.

There are two problems with this model: First, how can the high velocity flow escape the inner, high density region around IRC2? Dynamical friction with low velocity gas will decelerate high velocity clumps on a time scale  $t_D$  given by

$$\left[ \frac{t_D}{y} \right] \approx 0.2 \left[ \frac{n_{\text{cl}}}{n_0} \right], \quad (16)$$

where  $n_{\text{cl}}$  is the density in high velocity clumps which may be  $> 10^{10}\ \text{cm}^{-3}$ , and  $n_0$  is the density of the surrounding cloud which scales with radius as  $R^{-\alpha}$  ( $\alpha \approx 2$ ), and may reach  $10^9\ \text{cm}^{-3}$  at about  $10^{15}\ \text{m}$  (for a discussion of the density profile, see Downes *et al.* 1981). Hence, dynamical time scales are always shorter than  $t_D$  in the outer part of the source ( $R > 10^{16}\ \text{cm}$ ,  $n_{\text{cl}} \gg n_0$ ), and high velocity clumps can easily escape. In this case, the lifetime of high velocity  $\text{H}_2\text{O}$  features will depend more critically on the hydrodynamical stability (and the pumping) of the cloudlets (e.g., Genzel

*et al.* 1979a; Norman and Silk 1979). In the very inner part of the source ( $R \sim 10^{14} - 10^{15}$  cm), however, dynamical lifetime and deceleration time may become comparable. The high velocity clumps may still be able to escape if there is a flattened distribution of the high density material with the high velocity flow escaping at the poles (see Elmegreen and Morris 1979).

The second problem with this picture lies in the observed double-packed profile of the SiO "shell features." Such a profile would be expected only for smooth radial flow with low turbulence and small velocity gradients (e.g., Genzel *et al.* 1980). The interaction of a high velocity wind with a surrounding cloud, however, probably would create a very turbulent boundary layer (Elmegreen 1978; Elmegreen and Morris 1979).

#### V. INTERPRETATION OF THE MASERS

The H<sub>2</sub>O data and the new high-resolution infrared maps indicate that there are three different types of H<sub>2</sub>O masers in the Orion-KL region: the H<sub>2</sub>O "shell features," low velocity features, and high velocity features.

The H<sub>2</sub>O "shell features" associated with the 18 km s<sup>-1</sup> flow in the immediate vicinity of IRC2 resemble the double-peaked OH maser profiles from expanding circumstellar envelopes in late-type stars. Most of these features have not significantly changed in radial velocity or intensity in the past 10 years (Sullivan 1973; Hansen 1980). Their apparent sizes of  $5 \times 10^{14}$  to  $5 \times 10^{15}$  cm are larger than any of the other H<sub>2</sub>O masers in the Orion region by at least an order of magnitude. The emission probably occurs along fixed paths through the expanding envelope of IRC2 where conditions are favorable for maser amplification. From their apparent size and spatial distribution on VLBI maps (Hansen 1980), these masers are located at  $10^{15} - 10^{16}$  cm from IRC2. At this radius, the radiation may have an equivalent blackbody temperature of 300–1000 K and a maximum flux near the 2.7 and 6  $\mu$ m vibrational bands of H<sub>2</sub>O. The H<sub>2</sub>O "shell features" might, therefore, be radiatively pumped through the vibrational bands of the molecule (Deguchi 1977).

The low velocity masers in the Orion-KL region also have very stable radial velocities. Despite variability in intensity, individual masers have a lifetime of more than 10 years. The variability, and, in particular, the dramatic increase in flux density of a feature at 8.1 km s<sup>-1</sup> (LSR) by 3 orders of magnitude to  $> 10^6$  Jy (Abraham, Opher, and Rafaelli 1979) may indicate that the low velocity H<sub>2</sub>O masers are not radiating isotropically. The flux density from a saturated cylindrical maser of length  $l$  and pump rate  $P$  is proportional to  $Pl^3$  (Goldreich and Keeley 1972). To explain the flare in Orion, a change in the pump rate  $P$  of 3 orders of magnitude or a change in  $l$  of 1 order of magnitude

would be required. The 20  $\mu$ m data presented by Downes *et al.* (1981) were taken during the flare-up but do not show any sign of enhanced infrared emission at the position of the flaring feature. (Otherwise, there is a good positional correlation between masers and infrared emission.) The flare-up may have been caused by the maser "beam" happening to point in our direction, thereby changing the effective maser length  $l$  by factors of  $\sim 2-10$ , depending on the degree of saturation.

The proper motions show that the low velocity masers in Orion are probably dense cloudlets of gas moving along with the 18 km s<sup>-1</sup> flow. These masers may be dense condensations formed from instabilities as the 18 km s<sup>-1</sup> flow encounters "stationary" clouds in the KL Nebula. The kinetic temperature as well as the dust temperature in the 18 km s<sup>-1</sup> flow may be 100–200 K (Phillips *et al.* 1977; Downes *et al.* 1981). The most likely pumping mechanism for these masers may therefore be radiative or collisional pumping of the rotational levels of H<sub>2</sub>O. The mechanism for the formation of the masers, as well as a collisional or radiative pump, also might explain the good correlation of clusters of low velocity H<sub>2</sub>O masers with the 20  $\mu$ m condensations.

The high velocity H<sub>2</sub>O masers in Orion-KL are highly variable, and individual features persist for only a few years. They are typically 1–2 orders of magnitude weaker than the low velocity features, but their apparent diameters measured with VLBI are also smaller than those of low velocity features, by factors of 3–10. Hence, in most cases the brightness temperatures of high and low velocity masers are comparable. Like the low velocity features, high velocity features probably represent moving clumps of high density material. The high velocity masers are most likely pumped collisionally, possibly by their own deceleration in the surrounding dense molecular cloud.

#### VI. CONCLUSIONS

We have demonstrated that the observed changes in relative positions of H<sub>2</sub>O maser features are probably caused by *kinematic motions* of the maser cloudlets. From a statistical comparison of transverse and radial motions of many maser features in a given source, one can determine the *distance* of the maser source to better than  $\pm 20\%$ . This provides a new *primary* method of determining distances to star forming regions throughout our Galaxy. When clock and baseline calibrations are improved, it will be possible to attain relative positional accuracies of a few micro-arcsec and to measure distances to some of the extragalactic H<sub>2</sub>O masers (Churchwell *et al.* 1977; Lepine and Marques Dos Santos 1977; Huchtmeier *et al.* 1978).

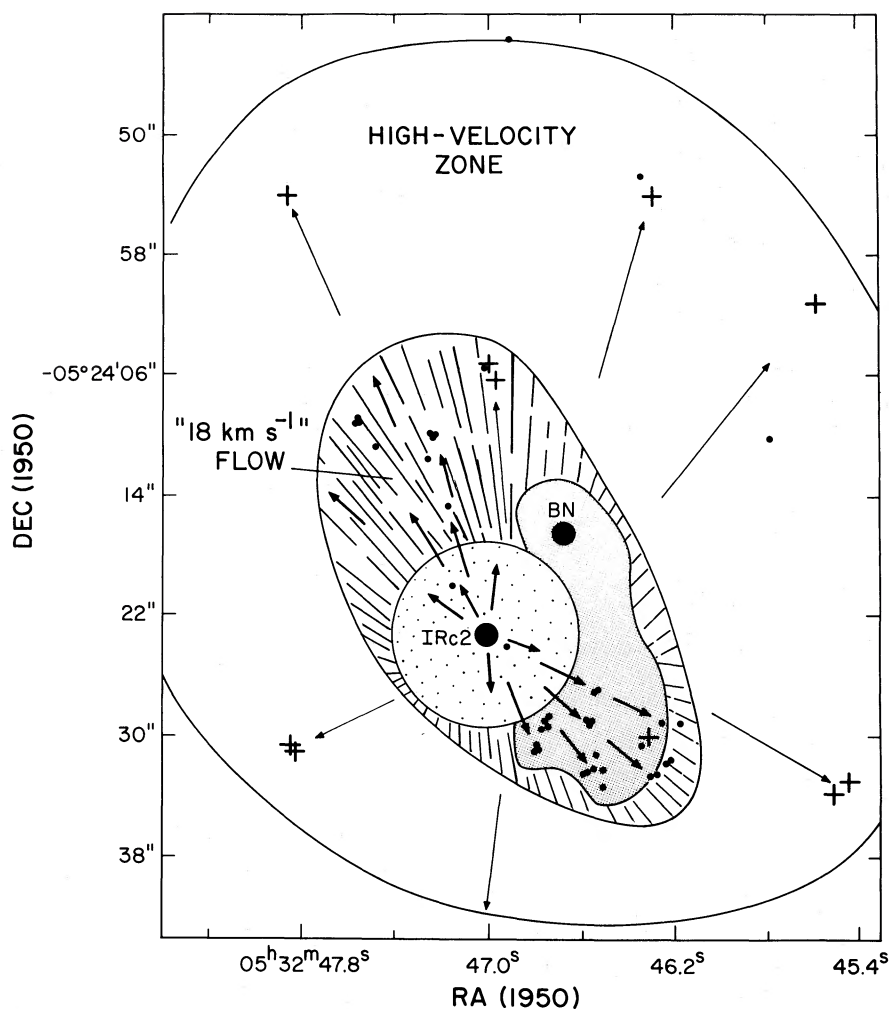


FIG. 8.—Schematic model of the Orion-KL outflow. Indicated are the  $18 \text{ km s}^{-1}$  zone (oval) and high velocity zone (outer line) around IRC2. Black dots are the  $\text{H}_2\text{O}$  low velocity masers and crosses denote the  $\text{H}_2\text{O}$  high velocity masers. The stippled region around IRC2 is the central part of the  $18 \text{ km s}^{-1}$  flow, where the high excitation molecular “plateau” lines ( $\text{SiO}$ ,  $\text{SO}_2$ , etc.) may originate. The “plateau” emission from  $\text{CO}$  and  $\text{NH}_3$  probably come from the oval outer region of the  $18 \text{ km s}^{-1}$  zone. The densely stippled region is the central part of the Kleinmann-Low Nebula which may contain very dense quiescent gas. The ammonia “hot” core and the  $20 \mu\text{m}$  compact features (IRC3, IRC4, IRC5, etc.) are located here and may show the effects of an interaction of the flow with the dense quiescent gas. In this model, the Becklin-Neugebauer object (BN) is also associated with the region and may be located behind the approaching side of the  $18 \text{ km s}^{-1}$  flow.

The proper motion data in Orion-KL support an interpretation of the KL Nebula (Fig. 8) in which the compact infrared source IRC2, and not the BN object, is the dominant energy source and the origin of the outflow phenomena observed in molecular lines. IRC2 has a luminosity of  $10^4$ – $10^5 L_\odot$  and is heavily obscured at near-infrared wavelengths by its own large mass loss. The mass loss in the  $18 \text{ km s}^{-1}$  flow is about  $10^{-2}$  to  $10^{-4} M_\odot \text{ yr}^{-1}$  and has been continuous over the past  $10^3$ – $10^4$  years. The  $18 \text{ km s}^{-1}$  flow (stippled and oval regions in Fig. 8) can be followed from  $10^{14}$  cm to  $2 \times 10^{17}$  cm from IRC2, in the maser lines of  $\text{SiO}$ ,  $\text{H}_2\text{O}$ , and  $\text{OH}$ , and the high excitation lines of  $\text{NH}_3$ ,  $\text{CO}$ , and  $\text{HCN}$ . In addition to the  $18 \text{ km s}^{-1}$  flow, there

is a second outflow at higher velocities ( $30$ – $100 \text{ km s}^{-1}$ ) that probably has a lower mass loss rate ( $\gtrsim 10^{-5 \pm 1} M_\odot \text{ yr}^{-1}$ ). The high velocity flow extends out to about  $3 \times 10^{17}$  cm in radius (outer zone in Fig. 8) and can be observed in the high velocity  $\text{H}_2\text{O}$  masers, the near-infrared lines of molecular hydrogen and the microwave lines of many molecules ( $\text{CO}$ ,  $\text{HCO}^+$ ,  $\text{HCN}$ , etc.). The high velocity flow could come from a second source, such as BN, but it is more likely associated with IRC2. The mass loss of IRC2 may be variable, or both the high velocity flow and the  $18 \text{ km s}^{-1}$  flow might be driven by a fast stellar wind from IRC2.

The outflow has a large influence on the dense, inhomogeneous surrounding molecular cloud and vice

versa. The "hot" ammonia core, the enhanced density of H<sub>2</sub>O masers at the core of the KL-Nebula, and the compact and extended near-infrared components may all be manifestations of this intense interaction. These clumps need not contain stars of their own, as previous infrared papers have suggested. The infrared data require only two hot stellar objects in the KL region, namely BN and IRC2.

Orion-KL is probably not unique. Observations of H<sub>2</sub>O masers show the phenomena of low and high velocity emission in regions of star formation throughout the Galaxy, and the proper motion data in W51MAIN and W51NORTH also show outflow of material from a central source (Papers II, III).

We are very grateful for all the help and cooperation provided in this long series of VLBI experiments by our colleagues, the technical and engineering staffs, and the operators of the different VLBI stations. We especially wish to thank L. R. Kogan, V. I. Kostenko, and L. I. Matveyenko of the Space Research Institute in

Moscow; I. G. Moiseev and I. Strepka of the Crimean Astrophysical Observatory; J. Eıldér, E. Kollberg, B. Rönnäng, and O. E. H. Rydbeck of the Onsala Space Observatory; A. Downes, W. Harth, R. Schwartz, Warwick Wilson, and W. Zinz of the Max Planck Institute for Radio Astronomy; J. C. Carter and A. E. E. Rogers of the Haystack Observatory; R. Lacasse and R. C. Walker of the National Radio Astronomy Observatory; B. F. Burke of the Massachusetts Institute of Technology; K. J. Johnston of the Naval Research Laboratory; and A. D. Haschick, S. Rosenthal, and M. Schneps of the Harvard-Smithsonian Center for Astrophysics. Onsala Space Observatory is operated by the Research Laboratory of Electronics, Chalmers University of Technology, Gothenburg, with financial support from the Swedish National Science Research Council and the Swedish Board for Technical Development. Radio astronomy research at Haystack Observatory of the Northeast Radio Observatory is supported by the National Science Foundation.

## REFERENCES

- Abraham, Z., Opher, R., and Rafaelli, J. C. 1979, *IAU Circ.*, No. 3415.
- Baud, B., Bieging, J. H., Plambeck, R., Thornton, D., Welch, W. J., and Wright, M. 1980, in *IAU Symposium 87, Interstellar Molecules*, ed. B. Andrew (Dordrecht: Reidel), in press.
- Beckwith, S., Persson, S. E., Neugebauer, G., and Becklin, E. E. 1978, *Ap. J.*, **223**, 464.
- Burdjuzha, V. V., Charugin, V. M., and Tomosov, V. M. 1979, *Astr. Ap.*, **79**, 306.
- Churchwell, E., Witzel, A., Huchtmeier, W., Pauling-Toth, I., Roland, J., and Sieber, W. 1977, *Astr. Ap.*, **54**, 969.
- Clark, B. G. 1973, *Proc. IEEE*, **61**, 1242.
- Deguchi, S. 1977, *Pub. A. S. P.*, **29**, 629.
- Downes, D., and Genzel, R. 1980, in *IAU Symposium 87, Interstellar Molecules*, ed. B. Andrew (Dordrecht: Reidel), in press.
- Downes, D., Genzel, R., Becklin, E. E., and Wynn-Williams, C. G. 1981, *Ap. J.*, **244**, 869.
- Ebert, R., von Hoerner, S., and Temesvary, M. 1960, in *Die Entstehung von Sternen* (Hamburg: Springer Verlag).
- Elmegreen, B. G. 1978, *Moon & Planets*, **19**, 261.
- Elmegreen, B. G., and Morris, M. 1979, *Ap. J.*, **229**, 593.
- Fernandez, J. C., and Reinisch, G. 1978, *Astr. Ap.*, **67**, 163.
- Forster, J. R., Welch, W. J., Wright, M. C. H., and Baudry, A. 1978, *Ap. J.*, **221**, 137.
- Genzel, R., and Downes, D. 1977, *Astr. Ap. Suppl.*, **30**, 145.
- Genzel, R. et al. 1978, *Astr. Ap.*, **66**, 13.
- Genzel, R. et al. 1979a, *Astr. Ap.*, **78**, 239.
- Genzel, R., Moran, J. M., Lane, A. P., Predmore, C. R., Ho, P. T. P., Hansen, S. S., and Reid, M. J. 1979b, *Ap. J. (Letters)*, **237**, L73.
- Genzel, R., Downes, D., Schwartz, P. R., Spencer, J. H., Pankonin, V., and Baars, J. W. M. 1980, *Ap. J.*, **239**, 519.
- Genzel, R. et al. 1981, *Ap. J.*, in press.
- Giuffrida, T. S. 1977, Ph.D. thesis, Massachusetts Institute of Technology.
- Goldreich, P., and Keeley, D. A. 1972, *Ap. J.*, **174**, 517.
- Hall, D. B., Kleinmann, S. G., Ridgway, S. T., and Gillett, F. C. 1978, *Ap. J. (Letters)*, **223**, L47.
- Hansen, S. S. 1980, Ph.D. thesis, University of Massachusetts, Amherst.
- Haschick, A. D., Burke, B. F., and Spencer, J. H. 1977, *Science*, **198**, 1153.
- Hoyle, F., Solomon, P. M., and Woolf, N. J. 1973, *Ap. J. (Letters)*, **185**, L89.
- Huchtmeier, W. K., Witzel, A., Kühr, H., Pauling-Toth, I. I., and Roland, J. 1978, *Astr. Ap.*, **64**, L21.
- Kuiper, T. B. H., Rodriguez-Kuiper, E. N., and Zuckerman, B. 1978, *Ap. J.*, **219**, 129.
- Kwan, J., and Scoville, N. 1976, *Ap. J. (Letters)*, **210**, L39.
- Johnson, H. L., and Hiltner, W. A. 1956, *Ap. J.*, **123**, 267.
- Johnson, H. M. 1965, *Ap. J.*, **142**, 964.
- Larson, R. B., 1980, *M.N.R.A.S.*, **190**, 321.
- Lepine, J. R., and Marques Dos Santos, P. 1977, *Nature*, **270**, 501.
- Liszt, H. S., Wilson, R. W., Penzias, A. A., Jefferts, K. B., Wannier, P. G., and Solomon, P. M. 1974, *Ap. J.*, **190**, 557.
- Little, L. T., White, G. J., and Riley, P. W. 1977, *M.N.R.A.S.*, **180**, 639.
- Lüst, R., and Schlüter, A. 1955, *Zs. f. Ap.*, **38**, 190.
- Markowitz, W. M. 1949, *A. J.*, **54**, 111.
- Matsakis, D. N., Cheung, A. C., Wright, M. C. H., Askne, J. I. H., Townes, C. H., and Welch, W. J. 1980, *Ap. J.*, **236**, 481.
- Montes, C. 1977, *Ap. J.*, **216**, 329.
- Moran, J. M. 1976, in *Methods of Experimental Physics*, Vol. 12c, ed. M. L. Meeks (New York: Academic Press), p. 228.
- Moran, J. M., Johnston, K. J., Spencer, J. H., and Schwartz, P. R. 1977, *Ap. J.*, **217**, 434.
- Morris, M. 1975, *Ap. J.*, **197**, 603.
- Morris, M., Palmer, P., and Zuckerman, B. 1980, *Ap. J.*, **237**, 1.
- Nadeau, D., and Geballe, T. R. 1979, *Ap. J. (Letters)*, **230**, L169.
- . 1980, in *IAU Symposium 87, Interstellar Molecules*, ed. B. Andrew (Dordrecht: Reidel), in press.
- Norman, C. A., and Silk, J. 1979, *Ap. J.*, **228**, 197.
- Norris, R. P., Booth, R. S., and McLaughlin, W. 1980, in *Giant Molecular Clouds in the Galaxy*, ed. P. M. Solomon and M. G. Edmunds (Oxford: Pergamon Press), p. 193.
- Parenago, P. P. 1954, *Trudy Shternberg Astr. Inst.*, Vol. 25.
- Phillips, T. G., Huggins, P. J., Neugebauer, G., and Werner, M. W. 1977, *Ap. J. (Letters)*, **217**, L161.
- Radhakrishnan, V., Goss, W. M., and Bhandari, P. 1975, *Pramana*, **5**, 49.
- Reid, M. J. 1976, Ph.D. thesis, California Institute of Technology.
- Reid, M. J., Muhleman, D. O., Moran, J. M., Johnston, K. J., and Schwartz, P. R. 1977, *Ap. J.*, **214**, 60.
- Rieke, G. H., Low, F. J., and Kleinmann, D. E. 1973, *Ap. J. (Letters)*, **186**, L7.
- Rydbeck, O. E. H., Hjalmarsen, Å., Rydbeck, G., Eıldér, J., Sume, A., and Lindholm, S. 1980, in *IAU Symposium 87, Interstellar Molecules*, ed. B. Andrew (Dordrecht: Reidel), in

- press.  
 Schneps, M. *et al.* 1981, in preparation (Paper III).  
 Scoville, N. 1980, in *IAU Symposium 87, Interstellar Molecules*, ed. B. Andrew (Dordrecht: Reidel), in press.  
 ———. 1981, in *IAU Symposium 96, Infrared Astronomy*, ed. C. G. Wynn-Williams and D. Cruikshank (Dordrecht: Reidel), in preparation.  
 Strand, K. A. 1958, *Ap. J.*, **128**, 14.  
 Strelitskii, V. S., and Syunyaev, R. A. 1972, *Astr. Zh.*, **49**, 704; 1973, *Soviet Astr.—AJ*, **16**, 579.  
 Sullivan, W. T. 1973, *Ap. J. Suppl.*, **25**, 393.  
 Trumpler, R. J., and Weaver, H. F. 1953, *Statistical Astronomy* (New York: Dover), p. 336ff.  
 Walker, R. C., Johnston, K. J., Burke, B. F., and Spencer, J. H. 1977, *Ap. J. (Letters)*, **211**, L135.  
 Walker, R. C. *et al.* 1978, *Ap. J.*, **226**, 95.  
 Walker, R. C. *et al.* 1981, in preparation.  
 Wannier, P. G., and Phillips, T. G. 1977, *Ap. J.*, **215**, 796.  
 Wannier, P. G., Phillips, T. G., Huggins, P. J., and Knapp, G. R. 1980, *Bull. AAS.*, **11**, 705.  
 Werner, M. W., Gatley, I., Harper, D. A., Becklin, E. E., Loewenstein, R. F., Telesco, C. M., and Thronson, H. A. 1976, *Ap. J.*, **204**, 420.  
 Wilson, T. L., Downes, D., and Bieging, J. 1979, *Astr. Ap.*, **71**, 275.  
 Wright, A. E., and Barlow, M. J. 1975, *M.N.R.A.S.*, **170**, 41.  
 Wynn-Williams, C. G., and Becklin, E. E. 1974, *Pub. A.S.P.*, **86**, 5.  
 Zuckerman, B., Kuiper, T. B. H., and Rodriguez-Kuiper, E. N. 1976, *Ap. J. (Letters)*, **209**, L137.  
 Zuckerman, B., Palmer, P., and Morris, M. 1980, *Bull. AAS*, in press.

D. DOWNES: Institut de Radio Astronomie Millimetrique, B. P. 391, 38017 Grenoble Cedex, France, and Max Planck Institut für Radioastronomie, Auf dem Hügel 69, D53 Bonn, West Germany

R. GENZEL: Department of Physics, 563 Birge Hall, University of California, Berkeley, CA 94720

J. M. MORAN and M. J. REID: Harvard/Smithsonian Center for Astrophysics, 60 Garden Street, Cambridge, MA 02138